GSICS Global Space-based Inter-Calibration System

Quarterly

Newsletter – Summer 2015 Issue

Volume 9 Number 2
2015
doi: 10.7289/V5XK8CHN

Manik Bali, Editor

In This Issue

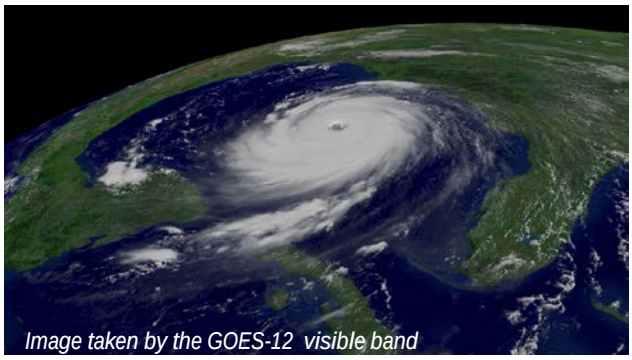

Image taken by the GOES-12 visible band

Sentinel-2A launched on 23rd June 2015 from French Guiana

An Integrated method to Improve the GOES Imager Visible Radiometric Calibration Accuracy

By Fangfang Yu and Xiangqian Wu, NOAA

Vicarious calibration, which uses not-on-orbit temporally stable reference targets, is often relied on to provide the post-launch calibration coefficients for the instruments without on-board calibration device. It is also used to validate the results from the on-orbit calibration studies.

For the solar reflective channels, more than one vicarious method is often applied to enhance the confidence to interpret the sensor in-orbit performance by cross-checking the calibration results. Multiple vicarious calibration methods have been examined at NOAA/NESDIS/STAR for GOES Imager visible data using various stable targets including Desert, Deep Convective Cloud (DCC), lunar, and stars as well as GEO-LEO ray-matched radiance pairs collocated over bright clouds. These various methods provide either the relative or absolute calibration, and are able to provide a temporal uncertainty of 2-4% over the sensor operational record. In this article, we introduce an integrated method, which is capable of combining multiple vicarious calibration methods to improve the relative radiometric calibration accuracy of the solar reflective channels. The details of the method can be found at Yu and Wu (2015).

Combination of vicarious calibration results

Three steps are applied to combine the results from different calibration methods: 1) apply the sensor degradation function to fit the time-series observations of each method, 2) normalize the monthly observations of each method to the value estimated from the degradation function to the first day of satellite operation (Day 1) using Equation 1, and 3) combine the normalized observations of each method as shown in Figure 1.

For GOES Imager visible data, the trending distributions of the four methods (desert, DCC, ray-matching and lunar irradiance) are very consistent, indicating that the impact of wavelength dependent degradation of the spectral response function, if any, is very small and negligible on the radiometric degradation with these methods. A common fitting function thus should exist among the combined observations for the sensor degradation trending.

$$Normalized\_Observation_t = \frac{S_{t,i}}{\hat{S}_{t=1,i}} \quad ...(1)$$

Where $S_{t,i}$ are the monthly observation of method *i* at time *t*; *t* is the time (in day or year) after the satellite became operation; $\hat{S}_{t=1,i}$ is the estimated observation for method *i* on Day 1.

Recursive filtering method to improve the relative calibration accuracy

The recursive filtering method is employed to determine the common fitting function for the combined normalizations. It is assumed that residuals of the fitting function are of Gaussian distribution and any deviation of the fitting residual beyond a pre-defined threshold can be considered as an outlier. This fitting and removal procedure is iteratively applied to the combined data until less than 3% of the observations are identified as outliers. The threshold in this study is defined as two-sigma value of the fitting residuals of each iterative loop. The result of selected observations from the combined method is shown in Figure 1. The relative calibration accuracy with the integrated method, after the removal of outliers, is 0.6% for GOES-12, improved from each individual one.

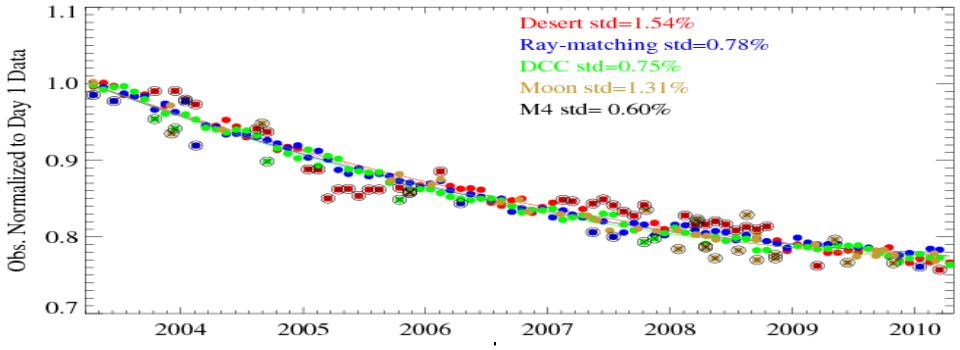

Figure 1: Combined time-series of reference observations from different vicarious calibration method, after normalizations to the estimated Day 1 values. The crossed observations are the outliers identified with the recursive filtering method.

Transferring relative calibration to absolute calibration

Two steps are involved to radiometrically scale the relative calibration with the integrated method to the Aqua-MODIS calibration reference. The first step is to reconstruct the time-series of pre-launch reflectance for the selected observations after recursive filtering using Equation 1; and then generate the absolute calibration correction coefficients using reflectance of reference targets with Equation 2. For GOES-12, DCC and the Sonoran desert are well characterized with Aqua MODIS Collection 6 (C6) data. We therefore use these two targets to implement the absolute calibration. It is found that there is less than 1% difference between the calibration coefficients derived with the DCC and desert reference targets.

$$Correction\_Coefficient_{t,i} = \frac{\mathrm{Re}\,f\_R_{t=1,i}}{R_{t,i}} * \frac{\hat{S}_{t=1,\mathrm{int}}}{\hat{S}_{t=1,i}} \quad ...(2)$$

where $\hat{S}_{i=1,\mathrm{int}}$ and $\hat{S}_{t=1,i}$ are the Day 1 observations estimated with the fitting functions for the combined normalizations after the recursive filtering and the normalized observations of method *i*, respectively. $R_{t,i}$ is the re-constructed pre-launch calibration at time *t* for method *i*. $\mathrm{Re}\,f\_R_{t=1,i}$ is the reflectance of reference target estimated with Aqua MODIS data for the method *i* at day *t*=1. Compared to the individual vicarious calibration method, the integrated method with the recursive filtering to remove outliers is able to improve the relative calibration accuracy and reduce the risk of capturing spurious sensor drift information caused by the variations or anomalous measurements of the reference target. For the near real-time data analysis, it will take almost two years to derive the stable coefficients for the trending function. It is expected that this integrated method will be useful to validate the GOES-R ABI on-board radiometric calibration accuracy for the solar reflective channels.

Reference:

Yu, F. and X. Wu, 2015. An integrated method to improve the GOES Imager visible radiometric calibration accuracy, Remote Sensing of Environment, 164, 103-113, http://dx.doi.org/10.1016/j.rse.2015.04.003.

Discuss the Article

Return to Page 1

doi: 10.7289/V5XK8CHN
GSICS Quarterly: Summer issue 2015 Volume 9, No. 2 2015

MODIS Terra-Aqua C6+ Cross-Calibration Improvements

By A. Lyapustin, X. Xiong, Y. Wang, G. Meister, S. Platnick, R. Levy, B. Franz, A. Wu, A. Angal, NASA

1. Introduction

MODIS observations of the Earth Observing System started in 2000 (Terra) and 2002 (Aqua). Of the two sensors, MODIS Aqua has been relatively stable with predictable on-orbit change, while response vs scan (RVS) and polarization sensitivity of MODIS Terra has been changing over time. Prior to Collection 6 (C6), MODIS calibration relied on trending of the Solar Diffuser and Moon at two specific angles of incidence (AOI) to characterize the RVS change. By the C6 timeframe, science analysis from the GSFC ocean biology processing group (OBPG) and MODIS aerosol group supported by MCST data provided evidence that the MODIS-Terra RVS change is non-linear and C5 calibration approach was not sufficient. The latest assessments of the calibration-related artifacts in MODIS Terra C5 products reveal global "decreasing" decadal trends of ~27% in aerosol optical thickness (AOT), ~17% in cloud optical thickness (COT), and ~0.01 in normalized difference vegetation index (NDVI) over land (*Lyapustin et al*., 2014).

To track RVS change, the MCST C6 algorithm introduced the Earth View monitoring of quasi-stable desert calibration sites in order to characterize all AOIs via trending of surface BRDF (*Sun, et al*., 2014). This approach improved RVS characterization and removed major trends of MODIS Terra. Yet, polarization sensitivity of MODIS Terra provided noticeable artifacts in geophysical retrievals. Figure 1 (left images) illustrates distortions in the atmospherically corrected surface reflectance (middle), and in $AOT_{0.47}$ (bottom) from algorithm MAIAC (*Lyapustin et al*., 2012) over Mid-Atlantic USA, DOY 349, 2012. The artifacts appear as 10- km stripes representing the residual scan mirror-side difference with effect maximized near the edge of scan.

For the land processing, we adopted polarization correction (PC) algorithm developed by OBPG (*Kwiatkowska et al*., 2008) using MODIS Terra-Aqua cross-calibration over the ocean. Figure 1 (right) shows that distortions disappear in the corrected image.

2. MODIS De-trending and Terra-Aqua Cross-Calibration Over Desert Sites

To study accuracy of C6 calibration with PC, we applied MAIAC processing to CEOS-recommended desert calibration sites using the time series (2000-2014) of MODIS data over 50×50km^2 subsets. Our analysis suggested that polarization correction of MODIS Terra should be limited to the blue part of spectrum (bands B3, B8-B10) (see *Lyapustin et al*., 2014).

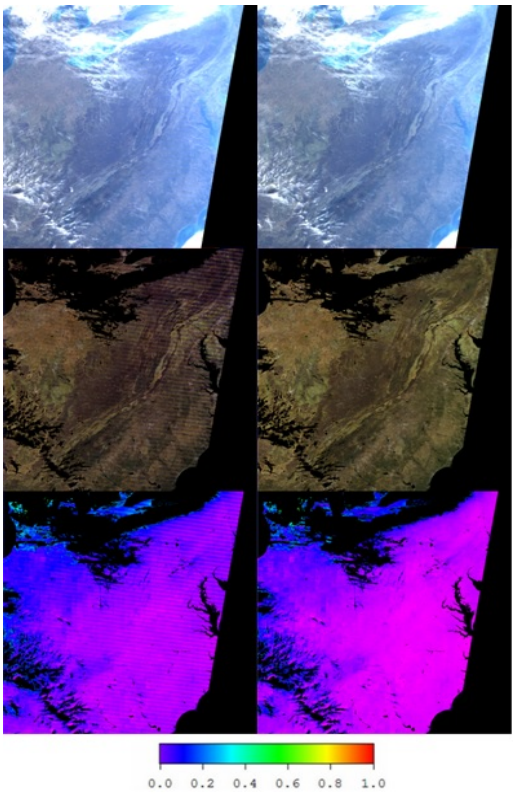

Figure 1. Improvements from polarization correction of MODIS Terra C6 L1B data (right) compared to uncorrected data (left) for day 349, 2012. PC removes 10- km striping in MAIAC $AOT_{0.47}$ (bottom) and spectral distortions in RGB surface reflectance (middle).

Bands	Egypt1	Libya1	Libya2	Libya4	Gain	σ
B1	1.017	1.023	1.021	1.019	1.020	0.0024
B2	1.004	1.008	1.007	1.006	1.006	0.0016
B3	0.989	0.992	0.992	0.990	0.991	0.0013
B4	1.006	1.013	1.010	1.009	1.009	0.0031
B8	0.997	0.996	0.998	0.994	0.996	0.0015

Table 1. Cross-calibration gain factor for four desert sites and average gain with respective standard deviation, σ

Return to Page 1

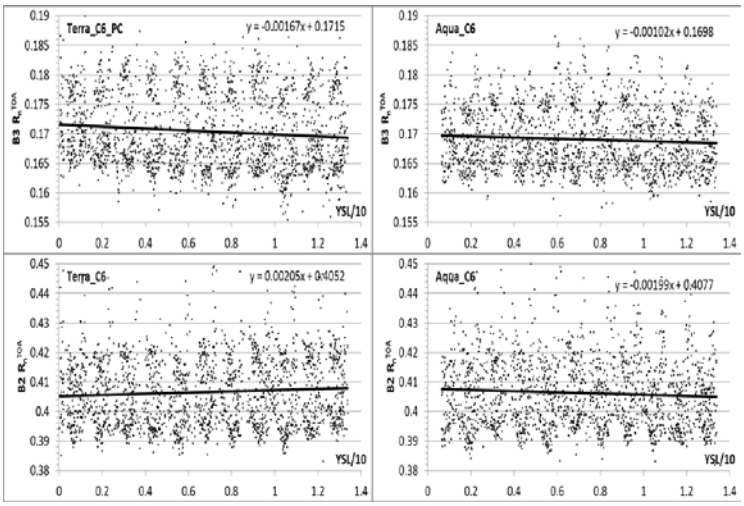

Figure 2. Clear-sky daily reflectance R_n^{TOA} over Libya4 site as a function of Years Since Launch (YSL)/10.

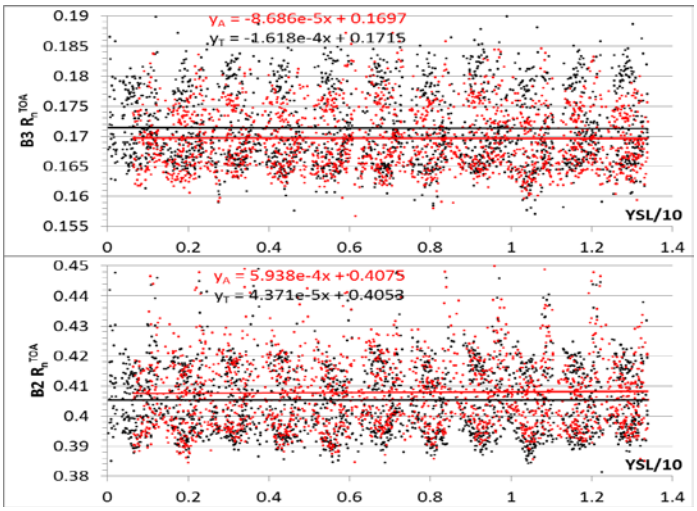

Figure 3. Clear-sky daily reflectance R_n^{TOA} over Libya4 site for MODIS Terra (black) and Aqua (red) bands B2 and B3 after de-trending.

To limit the effect of view geometry variability, we computed the expected top-of-atmosphere (TOA) reflectance (R_n^{TOA}) for the normalized view geometry (VZA=0°, SZA=45°) using MAIAC retrievals (cloud mask, column water vapor, aerosol properties, spectral surface BRDF). The time series of daily area-average R_n^{TOA} for Bands 3 and 2 is shown in Figure 2 where the left plots show C6 Terra (with PC for B3) and the right plots show C6 Aqua data. The TOA normalized reflectance R_n^{TOA} provides the de-trending (slope) coefficients for each band. This procedure has been applied to seven CEOS desert sites independently. We selected four sites (*Libya1*, *Libya2*, *Libya4*, *Egypt1*) which gave relatively similar trends (within a factor of 2-3 difference). Three other sites were excluded as providing much larger or unreliable trends. The final trend (slope per unit of reflectance per decade) was obtained as an average among four selected sites for Terra and Aqua separately. In the next step, we 1) used this value to obtain the new "de-trended" L1B dataset; 2) repeated MAIAC processing; 3) generated the new geometry-normalized R_n^{TOA} dataset. The "de-trended" R_n^{TOA} dataset is shown in Figure 3 for the same Bands 3 and 2.

Comparing Figures 2 and 3, one can see that this procedure effectively reduced the residual spectral trends by a factor of 5 to 10. With residual trends effectively removed, the R_n^{TOA} data, by virtue of geometric normalization, can now be used to obtain a cross-calibration coefficient between two MODIS sensors. This additional gain factor is applied to MODIS Terra since MODIS Aqua has been a better characterized and more stable instrument. As before, the gain coefficient is obtained as an average among the four selected sites. The summary of cross-calibration gain coefficients is provided in Table 1. As a result of this work, the calibration procedure has been extended beyond C6 L1B to include OBPG's polarization correction in bands B8-B10 and B3 (for MODIS Terra), de-trending (both sensors), and cross-calibration gain adjustment (MODIS Terra), which we further call C6+. MAIAC science analysis over the southern USA showed that C6+ improved agreement between Terra and Aqua decadal NDVI change by about a factor of 3 (*Lyapustin et al.*, 2014).). Currently, C6+ calibration is being used in the MODIS Land Discipline C6 re-processing.

References

Kwiatkowska, E.J., et al. (2008). Cross calibration of ocean-color bands from Moderate Resolution Imaging Spectroradiometer on Terra platform, *Appl. Opt.*, *47*(36), 6796-6810.

Lyapustin, A., Y. Wang, I. Laszlo, T. Hilker, F. Hall, P. Sellers, J. Tucker, S. Korkin, 2012: Multi-Angle Implementation of Atmospheric Correction for MODIS (MAIAC). 3: Atmospheric Correction. *Rem. Sens. Environ.*, http://dx.doi.org/10.1016/j.rse.2012.09.002.

Lyapustin, A., Y. Wang, X. Xiong, G. Meister, S. Platnick, R. Levy, B. Franz, S. Korkin, T. Hilker, J. Tucker, F. Hall, P. Sellers, A. Wu, A. Angal (2014), Science Impact of MODIS C5 Calibration Degradation and C6+ Improvements, *Atmos. Meas. Tech.*, 7, 4353-4365, doi:10.5194/amt-7-4353-2014.

Sun, J., X. Xiong, A. Angal, H. Chen, A. Wu, and X. Geng,2014. Time-Dependent Response Versus Scan Angle for MODIS Reflective Solar Bands, *IEEE TGRS*, vol. 52, issue 6, pp. 3159-3174

Discuss the Article

doi: 10.7289/V5XK8CHN
GSICS Quarterly: Summer issue 2015 Volume 9, No. 2 2015

Snow surface HDRF (BRDF) measurements at Dome C, Antarctica, for the inter-calibration and validation of satellite remote sensing products

By Amelia Marks (NPL), Corrado Fragiacomo (NIOG), Alasdair MacArthur (NERC Field Spectroscopy Facility), Giuseppe Zibordi (EC, JRC), Nigel Fox (NPL) & Martin King (Royal Holloway, University of London)

In-situ measurements of surface bi-directional reflectance distribution factor (BRDF) are required to convert satellite surface radiance measurements to an albedo. BRDF, experimentally determined as a hemispherical directional reflectance factor (HDRF), was measured at Dome C during the Australis Summer 2011- 2012 to support the inter-comparison and inter-calibration of satellite optical sensors. Dome C, Antarctica (75˚ S, 123˚ E) was suggested for surface HDRF measurements by Six et al., 2004 as the surface is flat, spatially homogeneous and temporally stable. The area also has very favourable atmospheric conditions. The measurements complement previous BRDF measurements performed at Dome C by Hudson et al, (2006) and show excellent agreement considering the very different measurement methodologies used.

The HDRF was measured using a Goino-RAdiometric Spectrometer System (GRASS), shown in Figure 1. GRASS records quasi-simultaneous, multi-angle, multi-spectral measurements of the Earth's surface reflected sun radiance. The full description of the system can be found in Marks et al. (2015), and Ball et al. (2015). GRASS consists of a hemispherical frame which is placed over a target surface. Radiance collectors are attached to arms running from the top to the base ring of the structure that can be rotated to cover 360˚ of azimuth. For the measurements

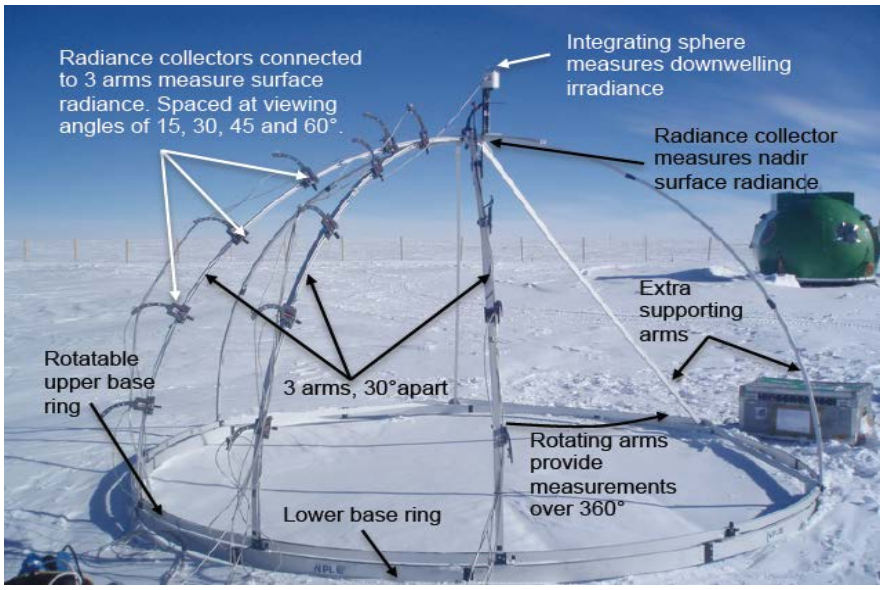

Figure 1: Set up of GRASS for Dome C HDRF measurements with 4 radiance collectors on 3 arms spaced 30˚ of azimuth apart. The arms of GRASS can be rotated 360˚ to record surface radiance at all azimuth angles.

at Dome C the radiance collectors were placed on three arms 30˚ of azimuth apart at viewing angles of 15, 30, 45 and 60˚, with a further radiance collector at nadir. The radiance collectors all focus on the same target area, with a viewing footprint varying from 0.049 to 0.141 m^2 and record the surface radiance in turn via fibre optics attached to a spectrometer, over the wavelength range 400 nm–1700 nm. Simultaneously with the surface radiance measurements, the downwelling irradiance is recorded via an integrating sphere to enable corrections for changes in illumination conditions.

Measurements of HDRF using GRASS were collected at eight sites along a linear ~100 m transect that was representative of the snowpack around Dome C and just east of the location used by Hudson et al. (2006). Hudson et al. (2006) took measurements of BRDF, reported as an anisotropic reflectance factor, at Dome C from the top of a 32 m tower with a viewing footprint from 70 to 1170 m^2. The method of Hudson et al. (2006) contrasts to GRASS as GRASS includes all azimuth angles in one measurement sequence and observes the same snow surface at each azimuth/viewing angle, within the limits of the varying small sensor footprint. The objective of the HDRF measurements with GRASS was to present independent angular reflectance measurements of the snow surface at Dome C performed with a methodology relying on simultaneous measurements of the same target surface with relatively small viewing footprints.

Return to Page 1

doi: 10.7289/V5XK8CHN
GSICS Quarterly: Summer issue 2015 Volume 9, No. 2 2015

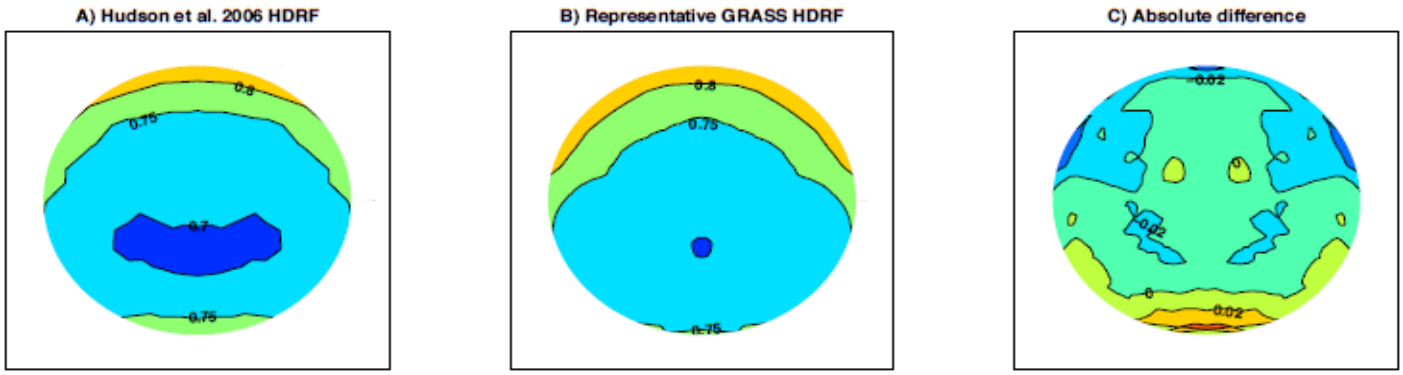

Figure 2: Comparison between HDRF measurements by Hudson et al. (2006) compared to HDRF measurements with GRASS at 1000 nm, taken at similar solar zenith angles. The solar principle plane runs vertically from the top to bottom of the plots.

A small viewing footprint enables small scale (<< 1 m) inhomogeneities in Dome C snow surface to be observed.

The HDRF measured at Dome C show that snow is forward scattering, as has been shown previously. Although, individual locations show distinct variance due to differences in surface structure of the snow. For example the forward scattering peak is much more evident at locations with a smoother snow surface. Spatial averaging of multiple HDRF measurements completed with GRASS produces HDRF values that are representative of current typical satellite sensor resolutions (with a ground sample distance of 10–100 m), and also enables comparison to Hudson et al. (2006) anisotropic reflectance factor measurements when converted to HDRF (using the method described in Marks et al., 2015).

Figure 2 shows a comparison of a polar contour plot at a wavelength of 1000 nm for HDRF values from Hudson et al. (2006) to the equivalent spatially averaged HDRF determined from GRASS. The agreement between Hudson et al. (2006) and GRASS spatially averaged HDRF measurements is very good. 95% of the viewing and azimuth angles compared exhibit less than a 4% relative difference and smaller viewing angles have less than a 2% difference. Both the measurements from GRASS and Hudson et al. (2006) show the snow is forward scattering, peaking in the forwards direction around values of 0.8 at a wavelength of 1000 nm. The agreement in the data sets adds strength to both the data presented here and those presented by Hudson et al. (2006), supporting the use of both data sets for current satellite inter-calibration and inter-comparison activities.

References

Ball, C, et al., 2015. Hemispherical-directional reflectance of windblown snow-covered Arctic tundra at large solar zenith angles. TGRS. 53, 10.

Hudson, S, Warren, S, Brandt, R, Grenfell, T., & Six, D., 2006. Spectral bidirectional reflectance of Antarctic snow: Measurements and parameterization. Journal of Geophysical Research, 111, 106.

Marks, A, et.al., 2015. Characterization of the HDRF (as a proxy for BRDF) of snow surfaces at Dome C, Antarctica, for the inter-calibration and validation of satellite remote sensing products. RSE, 407-416. Six,

Six, D, et. al., 2004. Surface characterisation of the Dome Concordia area (Antarctica) as a potential satellite calibration site, using Spot 4 Vegetation instrument. RSE, 89, 83-94

.

Discuss the Article

Return to Page 1

doi: 10.7289/V5XK8CHN
GSICS Quarterly: Summer issue 2015 Volume 9, No. 2 2015

VIIRS Day-Night Band destriping methods for improved uniformity

By Stephen Mills, Renaissance Man Engineering

Introduction

S-NPP VIIRS Day-Night Band (DNB) offers quantitative measurements of visible and near-infrared light over a dynamic range from full daylight to the dimmest nighttime scenes. This range presents a challenge to radiometric calibration such that striping and banding are still visible, day or night, but especially in low-light scenes. In order to improve imagery we have tested destriping algorithms that remove almost all striping from DNB imagery without reducing the overall radiometric accuracy for daytime, twilight and night. DNB calibration is complicated by the existence of 32 aggregation modes used across its scan, so the process must be done separately for each gain stage for each mode. We found that histogram equalization is effective for minimizing striping and banding. Stray light must be filtered out of the process, but improved uniformity is seen even in areas where stray light contamination exists.

Low-light detection capabilities of VIIRS DNB have opened up exciting areas of research. However, these new areas of investigation have pushed the usefulness of DNB data beyond the original design limits, so that striping has become a limiting factor. Areas include observation of city lights through thin clouds and haze; study of airglow; observation of clouds illuminated only by airglow; study of the auroras near the poles. All of these applications will benefit greatly by eliminating non-uniformities in the DNB radiance product.

VIIRS performs a cross-track scan of the Earth with its Rotating Telescope Assembly (RTA) that relays light to the DNB CCD array that is sectored into three stages to cover the 7-orders-of magnitude of dynamic range. These are: for day, the Low-Gain Stage (LGS); for twilight, the Mid-Gain stage (MGS) and for night, the High-Gain Stage (HGS) that uses TDI to boost the gain by a factor of 250. These three stages are on the same CCD and share a read-out integrated circuit, so electronic crosstalk is a problem among the three DNB gain stages, and this is believed to create nonlinearities that vary with detector, likely the root cause of striping.

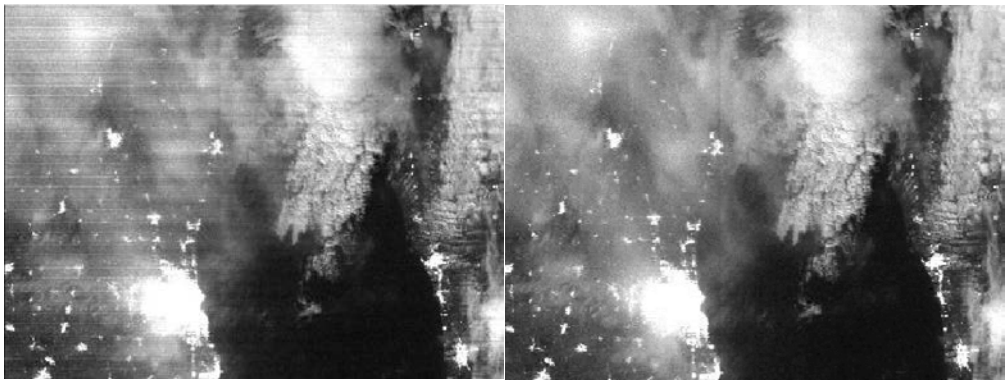

Figure 1: DNB image including Milwaukee & Lake Michigan, compares image with striping (left) and after destriping (right).

VIIRS uses three calibration sources: the Space-View (SV) for dark offset; the Black Body (BB) for thermal emissive gain; and the Solar Diffuser (SD) reflective gain. When viewing the calibration sources the DNB remains in a single aggregation mode per scan, unlike the earth view sector where the DNB is constantly cycling through the 32 aggregation modes to adjust the resolution. Because of the crosstalk, the calibration response is different from the earth view response and these differences contribute to the striping. Because of these differences, the SV cannot be used for determining the dark offset, and instead earth view data taken over the southern Pacific during a new moon is used.

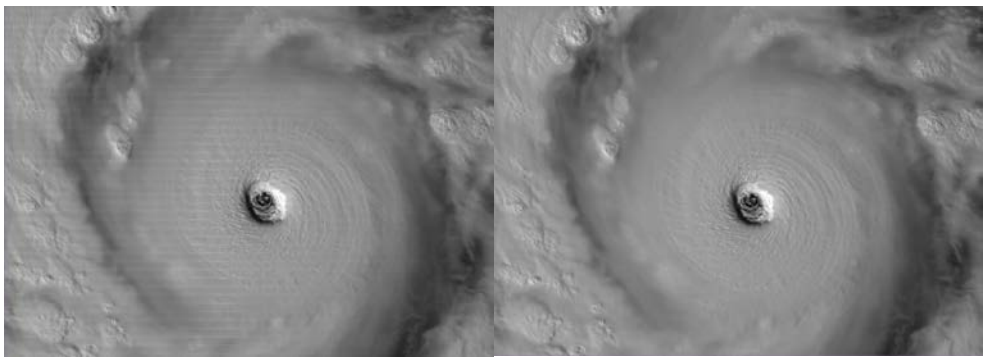

Figure 2: DNB image of Typhoon Vongfong, compares image with striping (left) and after destriping (right).

Return to Page 1

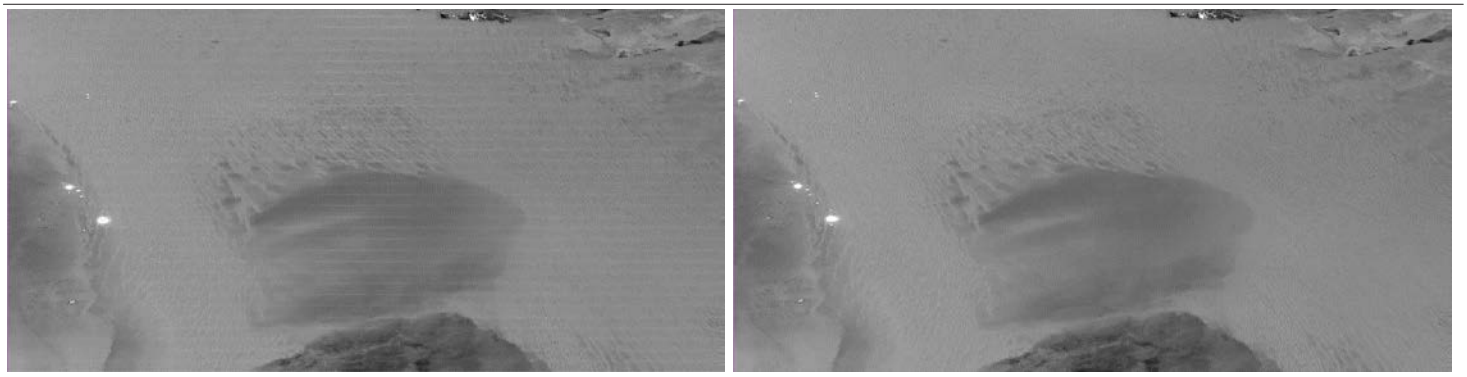

Figure 3. Libyan Desert, compares image with striping (left) and after destriping (right).

Also, when illuminated by the sun, SD data saturates for the MGS and HGS, so a special cross-calibration process using the earth view data is used instead. Crosstalk in these processes produced contribution to the striping seen in the DNB.

Methodology for Fixing DNB Striping

Calibration alone cannot fix striping because of inherent differences in response between earth and calibration views. Many destriping techniques have been developed for other sensors, and these all use the scene itself to maximize uniformity. If done correctly, radiometric uncertainty is not affected. However, the large dynamic range of the DNB presents a particular challenge. One technique tried was the moment matching. This determines for each detector variance and mean taken over many scenes. It minimizes difference in the moments among detectors by applying a scaling and offset. However, this method does not work well where there is a saturation limit or a lower limit as is the case for MGS and LGS, but it was used here for HGS destriping.

Histogram matching technique is an extension of moment matching, and takes cumulative histograms for each detector. Differences among the detector histograms are then minimized through scaling and offset. This can also be used to adjust for nonlinearities. Because this works for data that has saturation and/or a lower limit, it is used for MGS and LGS.

Examples These DNB images, plotted on a linear gray scale, compare before and after destriping. All are nighttime images from 10/07/2014 during a full moon. In all cases the destriping leaves no residual stripes.

- Figures 1 shows city lights, lighted roadways with light penetrating through the clouds and scattering, to creating a halo effect. The spread of the halo helps reveal the optical depth of the clouds and their structure and this can be seen more easily without striping. DNB has about 5 times better resolution than its heritage instrument, DMSP-OLS, and this has opened new areas of research involving anthropogenic lights at night. Destriping helps in taking full advantage of this.
- Figure 2 shows Typhoon Vongfong. Visible images of storms reveal structural features that are not seen in the emissive IR imagery. Without striping, reflectance combined with thermal emissive data in algorithms; help better understand these storm systems. The striped image was released to the press, but without the distraction of striping, it would have better conveyed the power of Vongfong.
- Figure 3 shows the Libyan Desert, known for being almost always clear and for its nearly uniform dunes, which is often used to validate satellite sensors for uniformity in reflective bands. Blowing dust and sand indicate wind direction and strength, only detectable at night using the DNB.

Acknowledgement

This work is funded by Renaissance Man Engineering.

References

Mills, S. and Miller, S., 2014, VIIRS Day-Night Band (DNB) calibration methods for improved uniformity, Proc. SPIE Vol. 9218, 921809, doi:10.1117/12.2060143.

Miller, S. et al., 2013, Illuminating the capabilities of the Suomi NPP VIIRS Day/Night Band, Rem. Sens., 5, 6717-6766.

Discuss the Article

doi: 10.7289/V5XK8CHN
GSICS Quarterly: Summer issue 2015 Volume 9, No. 2 2015

Adaptive Trending and Limit Monitoring Algorithm for GOES-R ABI Radiometric Parameters

By Zhenping Li, David Pogorzala, Ken Mitchell and J. Douglas, NOAA

The trending and monitoring of radiometric parameters are critical aspects of GOES-R Advanced Baseline Imager (ABI) operations for monitoring instrument health and safety and maintaining data quality. Given that radiometric parameters for GOES imagers typically exhibit a diurnal behavior, the existing trending approach of simply calculating the mean and standard deviation of a parameter's time series is not optimal. Instead the value of a parameter at a given time needs to be compared with its value at the same times in previous days to determine if the data are following a consistent diurnal trend. An Adaptive Trending and Limit Monitoring Algorithm (ATLMA) provides a new approach to trend and monitor radiometric parameters exhibiting the diurnal behavior.

The trending of a data set with a diurnal behavior becomes a data training process in ATLMA. The trend of a data set, $\{d_i\}$, with a diurnal behavior in ATLMA is expressed as a Fourier series,

$$f(t) = a_0 + \sum_{n=1}^{m}\left(a_n \cos\frac{2n\pi t}{24} + b_n \sin\frac{2n\pi t}{24}\right) \ldots(1)$$

where the time variable *t* has the unit of hours. The data training in ATLMA uses the least square fitting (LSQ) method obtain the parameters $\{a_n, b_n\}$ by fitting Eq. 1 to the existing data set. The resulting errors can characterized by the error, χ_i;

$$\chi_i = \mathrm{d}(t_i) - f(t_i) \quad .....(2)$$

and the noise σ_e, which is defined as

$$\sigma_e = \sqrt{\frac{1}{N}\sum_{i=1}^{N}\left(d(t_i) - f(t_i)\right)^2} \ldots(3)$$

The function $f(t)$ becomes the mean value for a variable independent of time, and the noise σ_e is the standard deviation for data set $\{d_i\}$. An outlier in such a limit-monitored data set is defined as any data point whose error value from the LSQ-fitted model is larger than a threshold, which is a user-defined multiple of the standard deviation obtained from the LSQ fit An iterative weighted fitting procedure is used in ATLMA data training so that the variable χ^2 is defined as

$$\chi^2 = \sum_{i=1}^{N}\left(f(t_i) - w_i d(t_i)\right)^2 \ldots(4)$$

The iterative fitting involves two steps. In the first step, the weight parameter, w_i, is set to 1.0 for every data point. After the first LSQ fitting is done, the noise level, σ_e, is calculated, and the weight parameter is defined based on the magnitude of the error of the data point. The new weight parameter for each data point can be defined with the following formula:

$$w_i = \begin{cases} 1.0, \ for\ |\chi_i| < 2.0\sigma \\ 1 - 0.125(|\chi_i| - 2.0\sigma)\ for\ 2\sigma \le |\chi_i| \le 10\sigma \\ 0\ for\ |\chi_i| > 10\sigma \end{cases} \quad .....(5)$$

The data point with larger error has less weight so that the parameters $\{a_n, b_n\}$ in Eq. 1 are not affected by the outliers. The simulation shows that the parameters $\{a_n, b_n\}$ become stable in the presence of outliers with the weighting function proposed in Eq. 5. With the new set of weights, a second LSQ fitting is performed. The outputs of these iterative LSQ fits are the parameters, $\{a_n, b_n\}$, and the noise level, σ_e. The error χ_i is recalculated for each data point, and compared to the threshold values defined by users. Figures 1 and 2 show an example of ATLMA data training for GOES13 imager calibration parameters. The training data set covers the data in two or three day period to avoid the daily fluctuations of the parameters $\{a_n, b_n\}$. The blue line in Fig. 1 represents the trend of the data set (in red) obtained from the ATLMA data training. The noise level obtained from the data training is used to determine the threshold for outliers in a data set. The trending is generally performed daily, and the daily changes in parameters $\{a_n, b_n\}$ and the residual noise level σ_e represent the long term trend of a data set. For example, noise level σ_e for the bias parameter in GOES Imager may provide the insight into the performance degradation in the corresponding detectors.

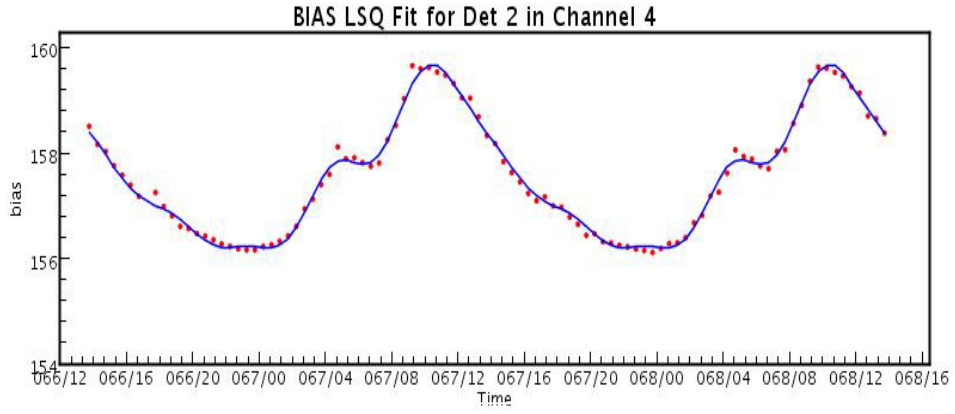

Figure 1 The ATLMA training for GOES13 channel 4 detector 2 bias parameters. The x-axis is time with the convention <DAYOFTHEYEAR>/<HOUROFTHEDAY> for the year 2015. The y-axis has the unit of GVAR counts.

Return to Page 1

doi: 10.7289/V5XK8CHN
GSICS Quarterly: Summer issue 2015 Volume 9, No. 2 2015

The ATLMA data training using recent data provides a predictive model, which includes the parameter set $\{a_n, b_n\}$ in Eq. 1 and the noise level. The model predicts the expected behavior for the The model predicts the expected behavior for the incoming data and determines if a data point is an outlier. The threshold for an outliers is defined as

$$S = N\sigma_e \quad .....(6)$$

where N is an user defined parameter. For a data point at time *t*, the data trend is calculated using Eq. 1 with the parameter set obtained from the data training with the most recent data. If the error defined in Eq. 2 is larger than the outlier threshold defined in Eq. 6, the data point becomes an outlier. Therefore, ALTMA enables the dynamic limit monitoring of new data, which provides users an instant feedback of any potential problem in real time or near real time. This makes it possible for much quicker response to anomalies. The same process for the real time data monitoring could be used in real time data filtering.

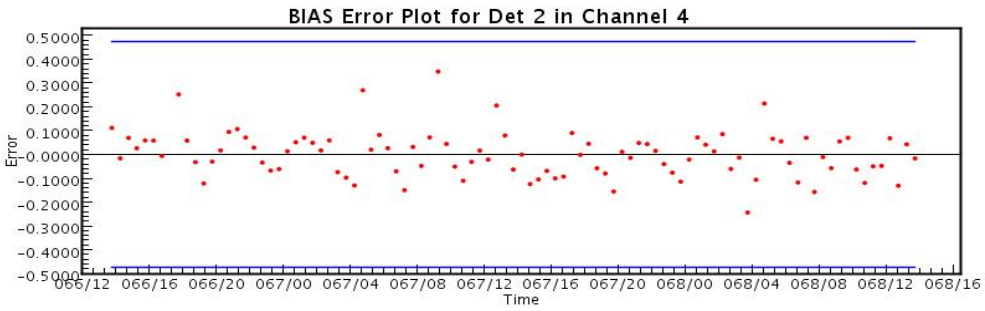

Figure 2 The errors for GOES 13 channel 4 detector 2. The blue lines are the outlier threshold, which is defined as 5 times of the noise level σ_e obtained from the ATLMA training. The x-axis is the time with the convention of <DAYOFTHEYEAR>/<HOUROFTHEDAY>.

If a data point becomes an outlier, it could also be replaced with the predicted value that are trained with the data from previous days.

This could be potentially very useful in GOES Imager data calibration process. For example, the space look data used in the calibration process are often contaminated by Straylight during the eclipse season, which leads to anomalous Imager calibration parameters in the infrared channels. The space look data contaminated by Straylight can easily be filtered out with the ATLMA data filtering, and replaced with the predicted values

ATLMA will be implemented in the forthcoming GOES-R ABI Radiometric Trending and Data Analysis Toolkit (GRATDAT) to assist in ABI radiometric performance monitoring and trending operations. It could potentially be used for the trending, limit monitoring and filtering of any spacecraft data with periodical behavior.

Discuss the Article

Quantifying uncertainty when comparing Space-based and Ground Observations

By Tony Reale, NOAA and Xavier Calbet, AEMET

A problem in satellite product cal/val is that uncertainty budgets are typically overlooked. Uncertainty originates in the native measurement space, for example the radiances from satellites or temperature from radiosonde observations (RAOB). Uncertainty is not solely an "intrinsic" property of the observations, but also has "secondary" components that are introduced when comparing measurements with different spatial and/or temporal characteristics including mismatch. Quantifying these components is needed for robust inter-comparison, validation and integration, for example, in WMO Integrated Global Observing System (WIGOS). Addressing such issues through strict comparison of reference RAOB, satellite IR/MW sounding

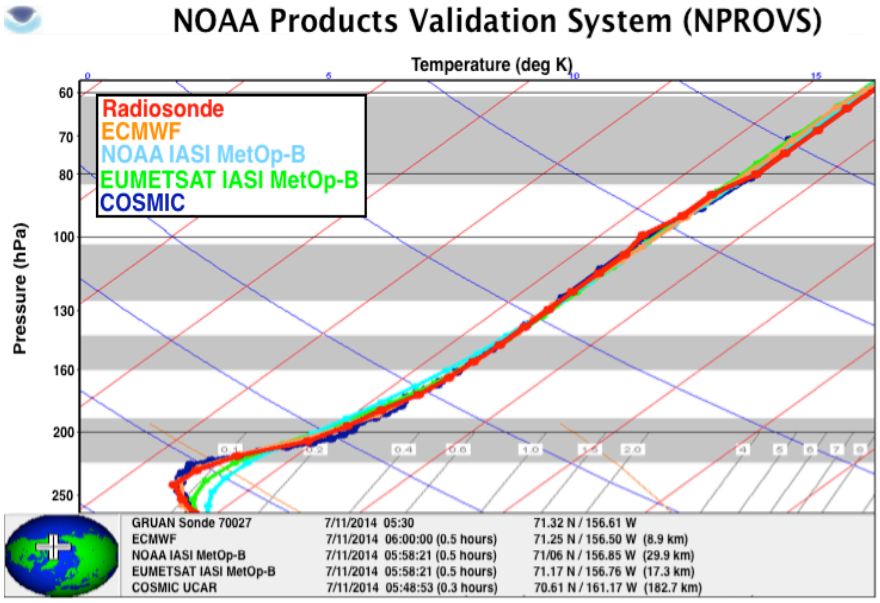

Figure 1: Collocated temperature profiles from GRUAN RAOB, COSMIC (Tdry), MetOp-B IASI soundings from NOAA and EUMETSAT and European Center for Medium-Range Weather Forecasts (ECMWF) analysis within 30 minutes and 30 km of RAOB except for COSMIC at 183 km.

Return to Page 1

and radio-occultation were targeted by the "3G" workshop convened by the World Meteorological Organization in May, 2014(see Page).
"3G" denotes the Global Climate Observing System (GCOS) Reference Upper Air Network (GRUAN) (www.gruan.org), Global Space-
based Inter-Calibration System (GSICS) and Global Navigation Satellite System Radio Occultation (GNSSRO).

Analysis to quantify these uncertainty components using GRUAN RAOB and derived temperature profiles from MetOp and GNSSRO Constellation Observing System for Meteorology, Ionosphere and Climate (COSMIC) (www.cosmic.ucar.edu) environmental satellites is presented. Even if intrinsic uncertainty estimates accompanied each set, which they usually do not, uncertainties introduced when comparing observations from different platforms can make them appear inconsistent. For example GNSSRO provide high vertical density line observations spanning over 150 km in the line of sight and vertically displaced about 150 km (stratosphere to surface) over 2 minutes. RAOBs provide a high vertical density of temperature point measurements vertically displaced upwards of 50 km over 100 minutes and downward looking radiometric satellite sounders measure layer averaged radiance over nominal thickness 2.5 km by 50 km with no vertical (nadir) or time displacement. Comparing these observations reduces to comparing a point, line and volume over variable measurement space.

This article provides an empirical view of the problem through direct comparison of collocated observations. Motivation stems from the "3G" Workshop goal to better coordinate interactions among the 3Gs in the context of WIGOS. An action from the meeting was to identify 3-way collocation datasets of GRUAN RAOB, GNSSRO and satellite Infra-red (IR) and Microwave (MW) sensors plus derived temperature profiles to characterize uncertainty across the geophysical, radiometric and RO spaces. Collocations windows for the RAOB and respective satellite sounders were +/- 1 hour

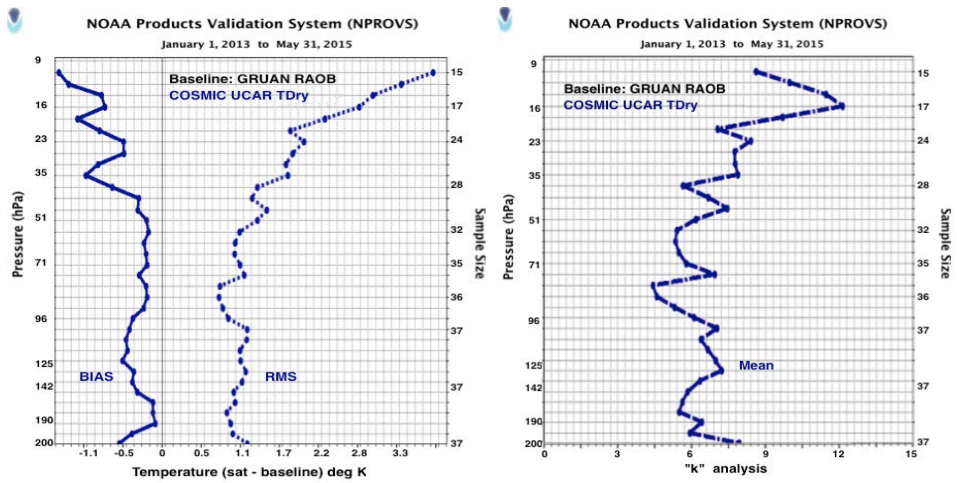

Figure 2: COSMIC Tdry-minus-RAOB T Bias and RMS error (left) and associated "k" profile analysis (right) above 200 hPa.

and 50 km and for GPSRO were +/- 3hr and 250 km. The source of collocations was the NOAA Product Validation System (NPROVS) operated at the Center for Satellite Applications and Research (STAR) (See Page).

Figure 1 shows a 3-way collocation of temperature profiles between 300 hPa and 50 hPa (SkewT /Log P thermodynamic diagram) for GRUAN RAOB, COSMIC and respective IASI MetOp-B processed by NOAA and EUMETSAT. Tdry (Sun et.al, 2013) is Shown for COSMIC and IASI profiles are successful, clear, retrievals. All profiles are within 30 minutes with the IR soundings (surface) within 30 km and the COSMIC (tangent point) within 183 km of the RAOB (surface). The collocation is at night and the agreement quite good with no differences exceeding 1.5 K. But are they good enough? Are they consistent?

The answer requires uncertainty estimates but only intrinsic uncertainty for GRUAN RAOB are routinely available. The GRUAN temperature uncertainty for Fig. 1 is typically on the order 0.10 K between 150 and 50 hPa, so any difference exceeding 0.2 K could be considered inconsistent. However, this does not account for the intrinsic satellite profile uncertainty and the uncertainty introduced when comparing profiles from different platforms. Equation 1 defines the GRUAN approach (Immler et al., 2010) for determining if two observations are consistent.

$$|m_1 - m_2| < k\sqrt{\sigma^2 + u_1^2 + u_2^2} \qquad \ldots(1)$$

where "u" designates intrinsic uncertainty, the subscripts 1 and 2 denote satellite and RAOB platforms, σ is the uncertainty introduced when comparing data from different platforms including mismatch and k =2 the threshold for consistency from Immler (2010).

Subsets of 2-way collocations of COSMIC and GRUAN profiles within 1 hour and 100 km are used to illustrate (1). Fig. 2 shows vertical profiles of COSMIC (Tdry)-minus-RAOB (T) Bias and RMS differences (left) and average "k" values (right) above 200 hPa. The "k" values are computed with the missing uncertainty components u1 and σ set to zero (0). Thirty-seven (37) collocations from six (6) mid-latitude/polar sites are analyzed. As seen, the "k" value for the 150 to 50 hPa layer hovers around six (6). This means that the quantity under the square-root must be increased a factor of nine (9) for k=2, the maximum value for consistent observations. Assuming that u1 is some multiple of u2 simplifies an estimation of the more elusive σ. For example setting u1 equal to u2, and substituting the mean u1 for the 18 profiles, approximately 0.15 K, yields an order of magnitude estimate of 0.40 K for σ over the layer. Given these, Fig. 2 suggests that 1.1 K RMS difference is within the margin of consistency for GRUAN RAOB and COSMIC temperature profiles collocated within one (1) hour and

100 km for the layer.

These results demonstrate analytical directions and a preliminary, order of magnitude estimate of σ for stratospheric temperature using carefully compiled collocation data. Such an approach, when extended to the radiance space, could help verify the radiance uncertainty from GSICS including against RT model calculations.

Better targeting of synchronized ground and space observations are needed and satellite products providers are encouraged to include uncertainty estimates. Meanwhile, collocations continue to accumulate at STAR.

References:

Immler, F.. J., et.al, 2010: Reference Quality Upper Air Measurements: guidance for developing GRUAN data products. *Atmos. Meas. Tech.*, **3**, 1217-1231, doi:10.519/amt-3-1217

Sun, B., et.al., 2013: Toward improved corrections for radiation-induced biases in radiosonde temperature observations. *JGR*, **118**, 4231-4243, doi:10.1002/igrd.5036

Discuss the Article

News in this Quarter

16th GSICS Executive Panel Meeting held in Boulder, USA on 15-16 May 2015

By Jérôme Lafeuille, WMO

The GSICS Executive Panel (EP) held its sixteenth meeting on 15 and 16 May 2015 in Boulder, Colorado, in advance of the 43rd annual meeting of CGMS. It was chaired by Peng Zhang of CMA and attended by representatives of CMA, EUMETSAT, ISRO, JMA, KMA, NASA, NOAA, USGS (remotely) and WMO, as well as the GCC, the GRWG Chair (remotely) and the two GDWG Co-chairs.

The Executive Panel noted the overall progress achieved by GSICS, which is having its tenth anniversary. The GSICS community is gradually encompassing all CGMS Members and GSICS proves to be a great collaboration and capacity building opportunity. Research is stimulated by an increasingly active GRWG. A data management infrastructure is in place. GSICS products are progressing in maturity and benefitting satellite data users, through improved calibration, assessments, and traceability to common references. Furthermore, recent commissioning operations of several satellites gave a striking demonstration of the practical value of GSICS for the satellite operators themselves. Through the use of GSICS methodology, references and tools they were able to efficiently identify anomalies such as stray-light effects, pre-launch calibration errors, and to monitor the long-term sensor performance degradation or the shift of Spectral Response Function.

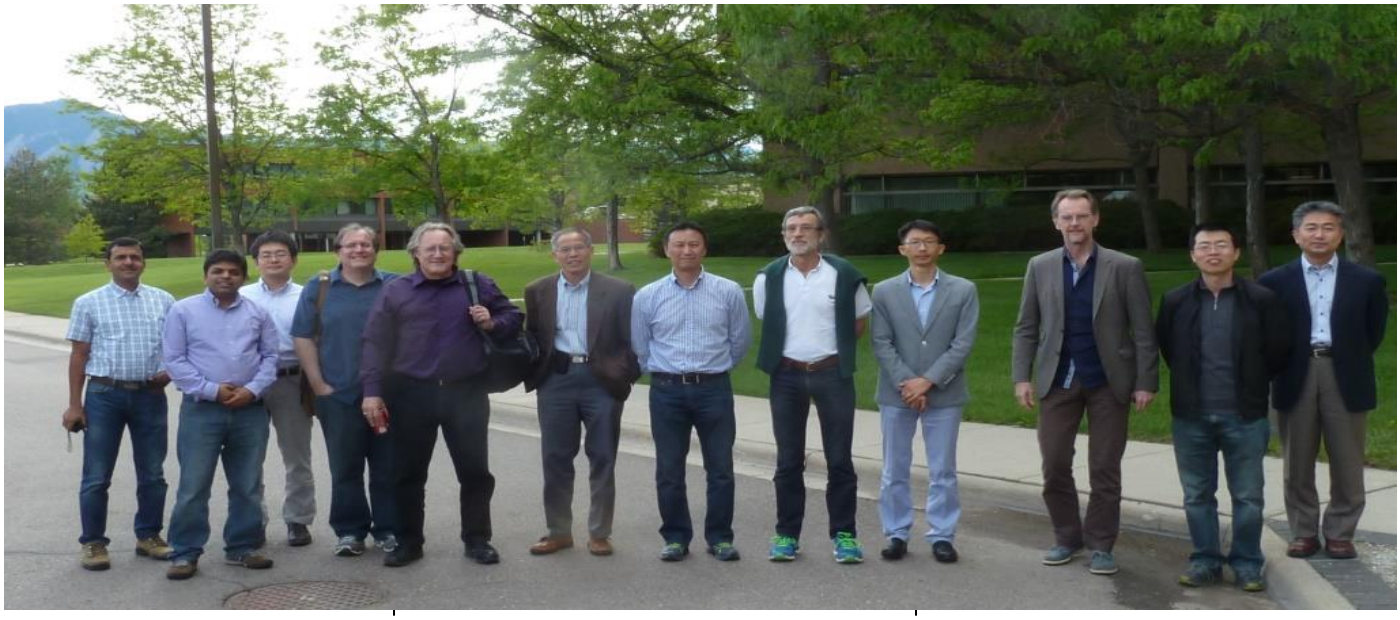

Above: Participants of the 2015 GSICS Executive Panel meeting. L->R Pradeep Thapliyal(ISRO), Manik Bali(NOAA), Masaya Takahashi(JMA), Mitch Goldberg(NOAA), James Butler(NASA), Xiaoxiong (Jack) Xiong(NASA) , Peter Miu(EUMETSAT), Jérôme Lafeuille(WMO), Kim Doheyong(KMA), Kenneth Holmlund(EUMETSAT), Peng Zhang(CMA) and Kazuo Umezawa(JAXA).

In order to reach a fully mature and operational stage, further steps need however to be taken. The promising results of solar channel calibration using DCC and/or the moon, and the on-going microwave activities need to be pursued and brought to the operational stage. But even for the infrared corrections, the first challenge we tackled with, the last mile from pre-operational to "operational" products is still to be covered.

In a broader perspective, our goal should be to make GSICS more visible,

better understood by potential users, and acknowledged as a building block of the WMO Integrated Global Observing System (WIGOS). The Executive Panel agreed that this requires transparent information on our objectives, structure, and activity. An updated set of GSICS Reference Documents should be available for our users, partners and stakeholders. GSICS has now published its Vision, and Terms of Reference. A top-level document is being prepared, which will replace the initial GSICS Implementation Plan. This documentation effort is not only a drafting exercise but triggers a fundamental reflection on the scope of GSICS, its deliverables, and the user requirements it aims to address.

The Executive Panel acknowledged the diversity of GSICS deliverables. While the "GSICS corrections" generated in near real-time are the ultimate result of GSICS, there is a wider range of outputs by which GSICS is useful to our external users (satellite data users) and/or internal users (satellite operators). GSICS deliverables include for instance calibration references and tools; standards and guidelines; monitoring results and assessments; intercalibration algorithms; routine correction products; and support services. A GSICS User Guide should be developed to explain how these various deliverables can be accessed, used and what review or approval mechanism they are subject to.

Another challenge is to formalize the user requirements basis of our work. Here we have to navigate between two pitfalls: on one side, users are often unable to express precise requirements for products which don't exist yet, on the other side they may express unrealistic requirements. One of our priorities for the coming year should be to collect and refine the GSICS User Requirements through a dialogue with representative users. This will be an important aspect of the GSICS User Workshop in Toulouse, in September.

The Panel agreed that, in collaboration with the CEOS Working Group on Calibration/Validation (WGCV), GSICS should bring a key contribution to the Architecture for Climate Monitoring from Space in defining a calibration infrastructure and key processes to ensure seamless continuity and consistency of climate records through accurate and homogeneous calibration.

Reacting on the reports of GCC, GRWG and GDWG after the successful joint meeting hosted by IMD in New Delhi in March, the Panel welcomed the concept of "prime correction" and the proposed strategy to select and use calibration reference sensors. It highly appreciated the EUMETSAT initiative to develop a GSICS Implementation of the ROLO model (GIRO) and supported the proposed approach to GIRO and GSICS Lunar Observation Dataset Usage Policy. It also recommended enhancing ground-based Moon observatories in order to reduce the uncertainty of absolute calibration by lunar observation. It approved the principle of long-term preservation of "GSICS Reanalysis corrections" and collocation data.

In reviewing the Terms of Reference of the GRWG and GDWG, the Executive Panel agreed that all satellite operators should participate in these Working Groups, and underlined that the substantial benefits of this participation required a substantial involvement, at the level of at least one man-month. Finally, the Panel unanimously designated Dohyeong Kim as new GRWG Chair, with Xiuqing (Scott) Hu and the outgoing Chair Tim Hewison as Vice-chairs. Bearing in mind the earlier designation of Peng Zhang as Executive Panel Chair, and Ken Holmlund as Vice-Chair, and Peter Miu and Masaya Takahashi as GDWG Co-chairs, Larry Flynn and Manik Bali as GCC Director and Deputy-Director, we can note a complete turn-over of GSICS leadership since its creation, with a spread of responsibilities across organizations and regions which is a good sign for such an international endeavour.

Discuss the Article

doi: 10.7289/V5XK8CHN
GSICS Quarterly: Summer issue 2015 Volume 9, No. 2 2015

Sentinel-2A launched on 23 June, 2015 from French Guiana

By Ferran Gascon and Bianca Hörsch, European Space Agency

The European Space Agency took a major leap forward on 23 June 2015 by launching the Sentinel-2A satellite from French Guiana. The Sentinel-2A is an important satellite of the Sentinel series of Earth Observation Satellites that are planned to be launched under the Copernicus program of the European commission. This satellite is equipped with a 13-channel Multi Spectral Instrument (MSI) that covers Visible, Near Infrared and Short Wave Infrared spectral domains. Placed in a Polar Sun Synchronous orbit, Sentinel-2A is a morning satellite (Equatorial crossing time of 10:30 AM). For the GSICS community it is interesting to note that this time is close to Landsat local time, hence gives possibility of in-orbit cross calibration between instruments on the two satellites.

Once in full operations, the Sentinel-2A provides a global coverage of land surfaces from 56 S to 84 N at a spatial resolution of 10m, 20m and 60m. Sentinel-2 observations of the earth has wide range of application, including Monitoring land cover and its change, Crop monitoring, retrieving vegetation indices (such as Leaf Area Index), Glacier monitoring, support to emergency monitoring and many more. The European Space Agency plans to launch an identical satellite, Sentinel-2B in late 2016 that would be placed 180 degrees apart/phased with the Sentinel-2A and will complete the constellation. The two instruments together will provide a global coverage with a 5-day revisit periodicity.

Figure: Sentinel-2A in orbit (Curtsey: ESA)

Sentinel-2 data will be available for download free and open from https://scihub.esa.int/ . Data access is currently planned to begin in October 2015. Further information on Sentinel-2 mission can be found at https://sentinel.esa.int or http://www.copernicus.eu/main/sentinels

Discuss the Article

Announcements

GSICS Users Workshop to be held on 22nd September 2015 in Toulouse, France

By Manik Bali, NOAA

The 2015 GSICS Users Workshop (GUW) will be held as part of the 2015 EUMETSAT Meteorological Satellite Conference. The Satellite conference will be held from 21 to 25 September in Toulouse, France and the GUW will be held on the afternoon of Tuesday 22nd September. This year the satellite conference is also collocated in space and time (not exactly!) with the SPIE European Remote Sensing Conference. Registration in advance is needed for participants for attending the conference and no registration fee would be charged for attending just the GUW. For additional information contact Tim.Hewison(AT)eumetsat.int

Return to Page 1

Joint GSICS GRWG-UVSG and CEOS WGCV-ACSG meeting to be held in College Park MD, USA, 8-9 October 2015

By Rosemary Munro(EUMETSAT), Lawrence E. Flynn(NOAA) and Bojan Bojkov(ESA)

A joint GSICS Research Working Group UV Sub-Group (GRWG-UVSG) and CEOS Working Group on Calibration and Validation Atmospheric Composition Sub-Group (CEOS WGCV-ACSG) meeting would be held in the vicinity of NOAA-NESDIS, College Park, MD, on the 8th and 9th October 2015.
The GSICS portion of this meeting would be held on 8th October 2015 while on the 9th October 2015 we have planned to discuss possible areas of common interest between GSICS, GRWG-UVSG and CEOS WGCV-ACSG. We would like to encourage participation from at least one calibration expert per relevant instrument (e.g. GOME-2, OMI, OMPS, SBUV/2, SBUS, TOU, TEMPO, SCIAMACHY, GEMS, S4/UVN, TropOMI, SAGE III, EPIC etc).
Please contact Lawrence E Flynn (Lawrence.e.flynn(AT)noaa.gov) for more information on the meeting.

Sixth WMO Workshop on the Impact of Various Observing Systems on NWP to be held in Shanghai, China, May 10-13, 2016

By Jérôme Lafeuille, WMO

The 6th WMO Workshop on the Impact of Various Observing Systems on Numerical Weather Prediction will be organized by the Inter Programme Expert Team on the Observing System Design and Evolution (IPET-OSDE) and will be hosted by the China Meteorological Administration at the headquarters of the Shanghai Meteorological Service in Shanghai, China, May 10-13 2016. Participants are expected from all the major NWP centers that are active in the area of impact studies.
With the ultimate goal to support the optimization of the observing effort, the Workshop will discuss the results of a range of studies evaluating the impact of specific components of the space and ground-based observing system, including observing system experiments (OSEs), adjoint and ensemble-based forecast sensitivity observation impact (FSOI and EFSOI), and estimates of analysis uncertainty.
In order to receive an invitation to participate in the workshop, you are invited to submit an abstract and title to the scientific organizing committee (SOC) via email to Dr. Lars Peter Riishojgaard, WMO Secretariat (lriishojgaard (AT) wmo.int) and Dr. Erik Andersson, ECMWF (erik.andersson (AT) ecmwf.int), by **15 November 2015**. Further information will be posted at http://www.wmo.int/pages/prog/www/WIGOS-WIS/meetings.html .

GSICS-Related Publications

Doelling, D. et al., 2015: The Radiometric Stability and Scaling of Collection 6 Terra-and Aqua-MODIS VIS, NIR, and SWIR Spectral Bands *TGRS* Vol. 53 No. 8 pp. 4520-4535

Isoz, O, S. A. Buehler, and P. Eriksson., 2015: Intercalibration of microwave temperature sounders using radio occultation measurements, *J. Geophys. Res. Atmos*., 120, 3758–3773, doi:10.1002/2014JD022699

Joel R. Norris and Amato T. Evan, 2015: Empirical Removal of Artifacts from the ISCCP and PATMOS-x Satellite Cloud Records. *J. Atmos. Oceanic Technol.*, **32**, 691–702. doi: http://dx.doi.org/10.1175/JTECH-D-14-00058.1

Kim, D. et al., 2015: Inter-comparison of the infrared channels of the meteorological imager onboard COMS and hyperspectral IASI data, *AAS* Vol. 32 No. 7 pp. 979-990: doi: 10.1007/s00376-014-4124-1

Liu, L. et al .,2014: Multitemporal cross-calibration of GF-1 WFV and Terra MODIS reflective solar bands SPIE PROCEEDINGS Vol. 9298

William B. Rossow and Joseph Ferrier, 2015: Evaluation of Long-Term Calibrations of the AVHRR Visible Radiances. *J. Atmos. Oceanic Technol.*,**32**, 744–766. doi: http://dx.doi.org/10.1175/JTECH-D-14-00134.1

Wu, A. et al., 2015: Sensitivity of Intercalibration Uncertainty of the CLARREO Reflected Solar Spectrometer Features TGRS Vol. 53 No. 9 pp. 4741-4751

Submitting Articles to GSICS Quarterly Newsletter:

The GSICS Quarterly Press Crew is looking for short articles (~800 to 900 words with one or two key, simple illustrations), especially related to cal/val capabilities and how they have been used to positively impact weather and climate products. Unsolicited articles are received for consideration anytime, and if accepted, will be published in the next available newsletter issue after approval/editing. Note the upcoming spring issue will be a general issue. Please send articles to manik.bali@noaa.gov.

With Help from our Friends:

The GSICS Quarterly Editor would like to thank Fangfang Yu for the lead article in this issue. Thanks are also due to Jerome Lafeuille, Fangfang Yu, Changyong Cao, Tim Hewison, Lawrence E Flynn and David Doelling for reviewing the articles.

Return to Page 1